Accuracy of automatic aerial triangulation with bundle block adjustment on large historical image blocks in mountainous terrain

Petra Brigitte Holden[1,2], Julian Smit[3]

[1] Plant Conservation Unit, Department of Biological Sciences, University of Cape Town, South Africa, petra.holden@uct.ac.za
[2]African Climate and Development Initiative, University of Cape Town, South Africa
[3] Geomatics Division, School of Architecture, Planning and Geomatics, University of Cape Town, South Africa

DOI: http://dx.doi.org/10.4314/sajg.v8i1.2

Abstract

Achieving accurate orthorectification is a major constraint to upscaling the use of historical aerial imagery for 20th century change detection. This paper presents a series of aerial triangulation bundle block adjustment post-processing model tests to determine the planimetric accuracy obtainable for large historical image blocks, which inherently contain film deformations e.g. warpage and shrinkage. Photo jobs with a range of photo numbers (12-237 images) and area coverage (>33 000-~150 000ha) were included. Self-calibration with 44-parameters and fixing the model to the ground control network achieved the highest final planimetric accuracy (total root mean square error [RMSE] ranging from 18.6 – 25.7px [7.1 – 21.8m] at ground control points and 20.5 – 27.7px [7.8 – 23.5m] at checkpoints). Allowing movement in the model by increasing standard deviations at ground control points or automating the removal of blunders in the model significantly reduced final planimetric accuracy. Removing automated points and running post-processing with no self-calibration also increased the error at checkpoint locations. This study shows that automatic aerial triangulation can assist towards reducing the number of ground control when orthorectifying large blocks of historical aerial photos. However, the study highlights the importance of post-orthorectification accuracy assessment because aerial triangulation accuracy results were not a correct reflection of the error in final orthoimages. Further work should focus on attempting to increase final planimetric accuracy by adjusting the accuracy and number of manual tie points and ground control in combination with altering the amount and positioning of automatic tie points.

Keywords: Photogrammetry; Historical aerial images; Orthorectification; Automatic orientation; Georeferencing; Aerial triangulation

1. Introduction

High-resolution aerial and satellite images are increasingly being used to evaluate and monitor a wide array of environmental and climatic variables (Chen et al. 2016; Bianchetti & MacEachren 2015). Despite recent advances, historical temporal and spatial coverage and poor resolution limits

the use of satellite images for determining landscape dynamics during the 20th century i.e. >30-80 years ago (Gennaretti et al. 2011).

Historical analogue aerial photos provide a unique opportunity to document 20th century landscape change (Abrate et al. 2013; Gennaretti et al. 2011; Ma & Buchwald 2012; Asiyanbola 2014; Palandro et al. 2003; Tekle & Hedlund 2000; Schiefer & Gilbert 2007). However, a major constraint to upscaling the use of historical aerial photos is challenges associated with accurately spatially referencing a large set of historical aerial images in order for them to be overlaid and/or quantitatively compared with other geographic datasets (Morgan, Gergel & Coops 2010; Rocchini 2004; Nagarajan & Schenk 2016; Wang & Ellis 2005a).

It is well described in the literature that topographically complex and highly mountainous areas present greater challenges for accurate spatial referencing than areas of flat and simple terrain (Rocchini & Di Rita 2005; Rocchini et al. 2012; Wang & Ellis 2005a, 2005b). Film or print shrinkage or warpage is another cause of geometric distortion and particularly of relevance to historic photographs and film (Morgan, Gergel & Coops 2010; Asiyanbola 2014). Errors associated with film deformations are independent to terrain roughness errors; however, these two sources of error combine in complex ways to have much larger impacts on planimetric accuracy (Morgan, Gergel & Coops 2010).

Current literature and country initiatives aimed at spatially referencing and geometrically correcting historical aerial images for change detection have mainly been driven through the standard procedures of manually locating an extensive number of ground control points that can also be located on an existing orthoimage or spatially referenced satellite image (Hughes, McDowell & Marcus 2006; Ma & Buchwald 2012; Nagarajan & Schenk 2016; Wang & Ellis 2005b). This includes approximately 4-20 ground control points per photo (or photo pair) or approximately 30-60 (or more) ground control points for approximately 10 000ha (Gennaretti et al. 2011; Hughes, McDowell & Marcus 2006; Abrate et al. 2013; De Rose & Basher 2011; Marignani et al. 2008; Pulighe & Fava 2013; Rocchini et al. 2006).

Automatic aerial triangulation with bundle block adjustment potentially provides an opportunity to increase the automation of orthorectification of historical aerial imagery and to reduce the amount of ground control required across a large set of aerial images (Addo 2010; Linder 2006). This is through automatic tie point image matching using feature based and least squares matching techniques, bundle block adjustment, and blunder removal (Chen et al. 2016; Verhoeven et al. 2012; Abrate et al. 2013; Addo 2010; Schenk 1996). However, the advantages of these methods for geometrically correcting historical aerial images have not been fully explored.

This paper presents an assessment of the potential for using digital automatic aerial triangulation with bundle block adjustment for orthorectifying damaged and degraded historical aerial images covering 30 000 – 150 000ha of mountainous and rugged terrain. The main aim of the paper is to describe the effects of different aerial triangulation post-processing models on final planimetric orthorectification accuracy with a reduced ground control network.

2. Materials and Methods

2.1. Study area

Automatic aerial triangulation post-processing model parameters were tested for a mountainous area in the Western Cape of South Africa known as the Groot Winterhoek Mountains (Figure 1). Historical aerial photos were sourced from South Africa's national mapping organisation, the National Geospatial Information (NGI) office, a Chief Directorate of the Department of Rural Development and Land Reform (DRDLR).

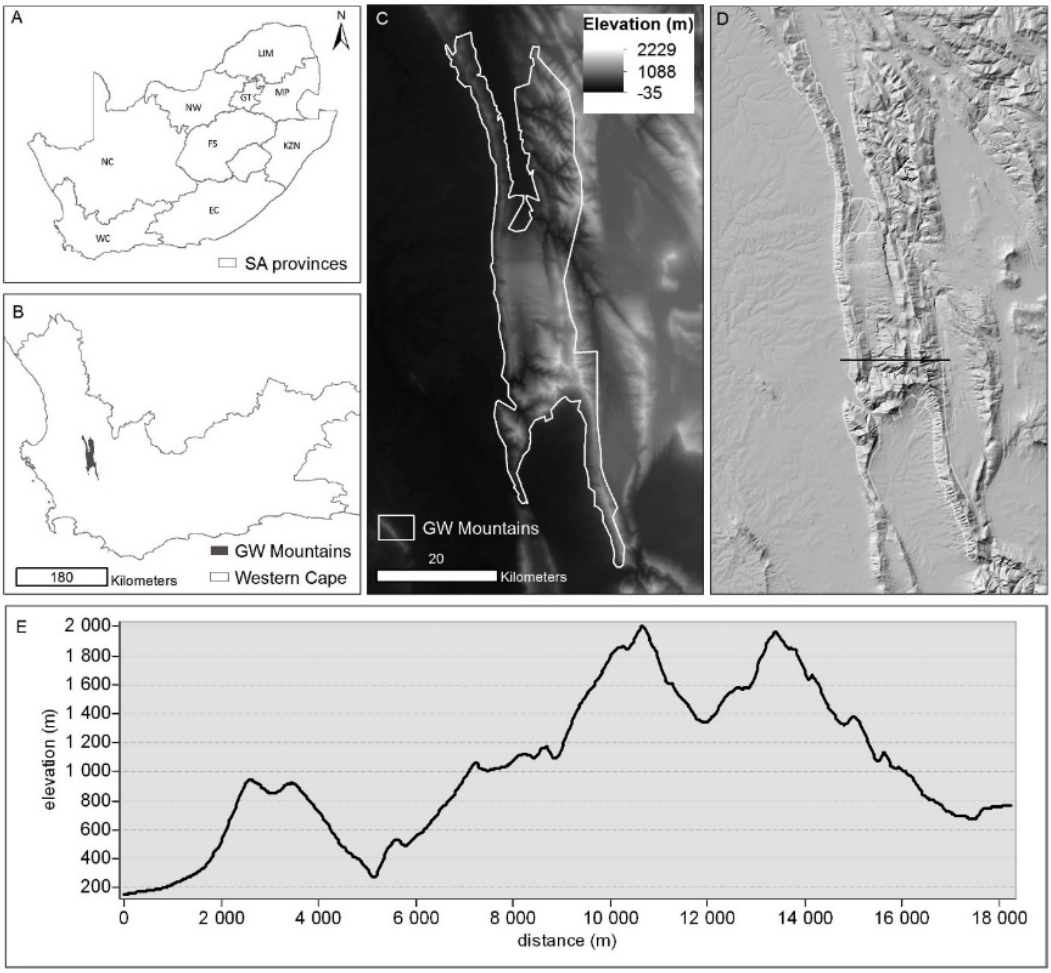

Figure 1 Study area: the Groot Winterhoek Mountains in the Western Cape (WC) of South Africa (A-E). E is linked to the horizontal line in D and is an indication of the complexity of the topography (NGI-DEM 2016; MDB 2013; DEA 2016; SUDEM 2014).

South Africa provides an ideal case study for this work as the NGI has an extensive collection of aerial photos dating from the early 1900s. Most of these have not been rectified because of technological, financial and institutional barriers as well as the limited awareness of the need and usage of such historical imagery (Figure 2).

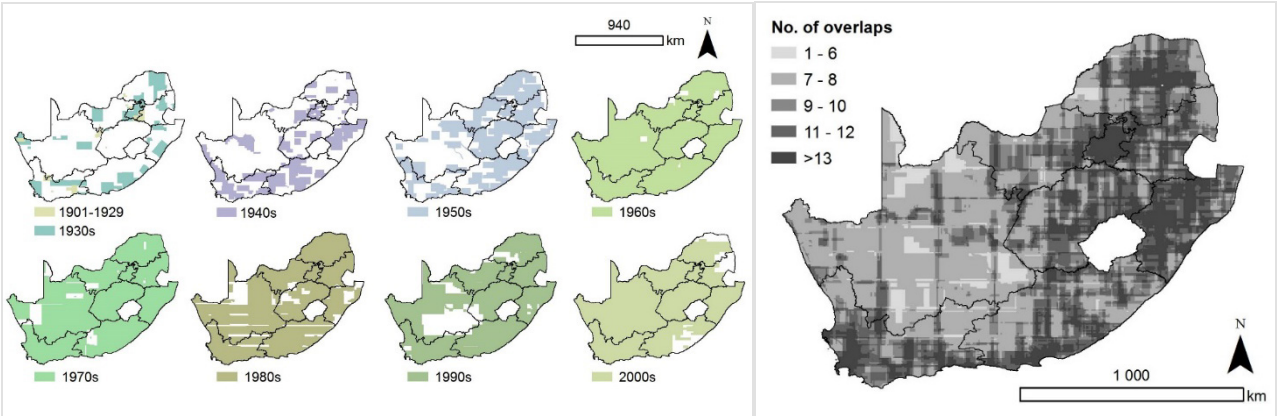

Figure 2 National coverage of non-rectified aerial imagery available for South Africa from the NGI with scales ranging from 1:5000 and 1:50 000. The image on the right shows the number of overlapping years (NGI (2015a, 2015b)).

2.2. Orthorectification and accuracy assessment

The study comprised four main components detailed in Figure 3. Aerial triangulation in the form of bundle block adjustment and orthorectification was conducted respectively using MATCH-AT and OrthoMaster within Applications Master from Inpho (Trimble/Inpho 2014). The final accuracy assessment of the orthoimages generated was manually determined using ArcGIS software (ESRI 2015).

2.2.1. Input: historical and reference data, images and DEM

High-resolution scans of historical aerial photo negatives (21 microns per pixel) and camera calibration reports were obtained from South Africa's National Geospatial Information (NGI) office for 1948/9 and 1971/2 (Table 1). The analogue film negatives were warped to different degrees and these film deformations were also visually evident after the scanning process.

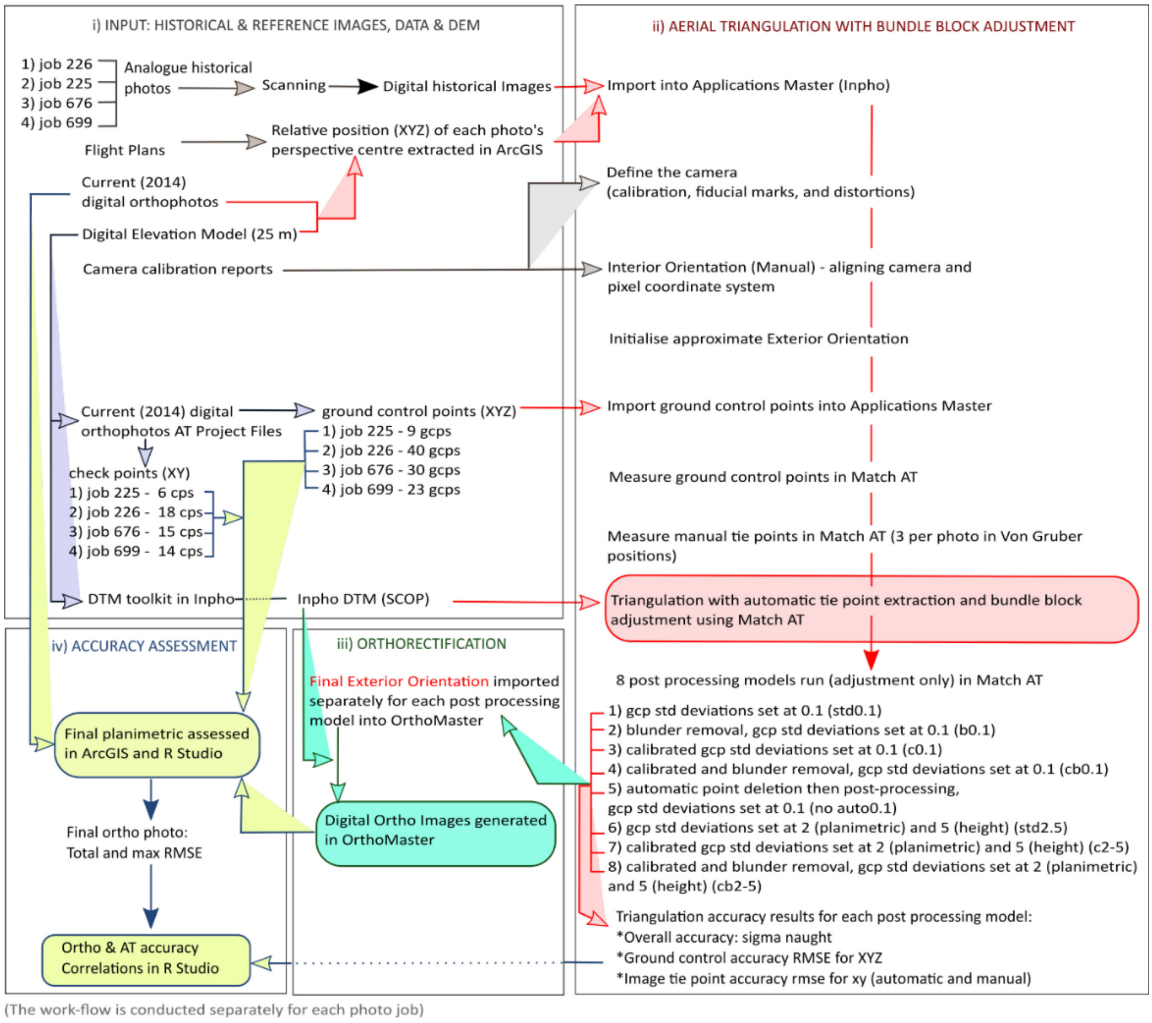

Figure 3 Study workflow consisting of four main components i) input images, data and DEM; ii) aerial triangulation with bundle block adjustment; iii) orthorectification; and iv) accuracy assessment.

Current 2013/2014 digital orthoimages were also obtained from NGI including the respective aerial triangulation project files (Intergraph project files) and a photogrammetrically compiled 25 m Digital Elevation Model (DEM) (absolute accuracy 2.5 – 5m) for use in the orthorectification process. Ground control points and Check points (XYZ) were measured directly from the current (2013/4) orthoimages' aerial triangulation Intergraph project. This was achieved by converting these files for use in Inpho and then using MATCH-AT to measure the coordinates for each respective ground control point. When placing a point in the existing orthoimages in MATCH-AT it provides the coordinates based on the block bundle adjustment used to generate the orthoimages. Ground control points were chosen based on their visibility across historical aerial photograph sets and the current orthoimages.

Table 1. Historical film based aerial photos including relevant scales and dates flown.

Job no.	Date flown	Scale	Area (ha)	No. of images (strips)	Focal length (mm)	Image size (cm)	No. of gcps[1]/cps[2]
225	Dec 1948	1:30 000	33 155	12 (5)	152.986	23*23	9/6
226	Jan-Feb 1949	1:18 000	156 800	237 (8)	152.986	23*23	40/18
676	Jan 1971	1:40 000	116 652	38 (8)	152.5	23*23	30/15
699	Feb 1972	1: 20 000	95 370	130 (7)	152.55	23*23	23/14

[1] *Ground Control Points: Directly used for aerial triangulation and bundle block adjustment to generate orthoimages.*
[2] *Check Points: Not used for aerial triangulation and bundle block adjustment but used to assess the consistency of planimetric accuracy across orthoimages generated.*

2.2.2. *Aerial triangulation with bundle block adjustment*

Aerial triangulation in the form of bundle block adjustment using a rigorous camera model was conducted to compute the exterior orientation of individual images. The rigorous camera model entails using physical parameters about the camera including focal length, principle point location, pixel size, and lens distortions and orientation parameters to represent the imaging geometry (Kaichang, Ruijin & Rong Xing 2003; Ma & Buchwald 2012). The rigorous camera model requires far less ground control points than rational function models which are generally appropriate for small areas with gentle terrain (Wang & Ellis 2005b). The bundled triangulation approach determines the exterior orientation using the collinearity condition (Nagarajan & Schenk 2016; Kaichang, Ruijin & Rong Xing 2003; Schenk 2004). Collinearity is expressed by the following equations:

$$x - x_o = -f \frac{a_{11}(X - X_s) + a_{12}(Y - Y_s) + a_{13}(Z - Z_s)}{a_{31}(X - X_s) + a_{32}(Y - Y_s) + a_{33}(Z - Z_s)} \quad [1]$$

$$y - y_o = -f \frac{a_{21}(X - X_s) + a_{22}(Y - Y_s) + a_{23}(Z - Z_s)}{a_{31}(X - X_s) + a_{32}(Y - Y_s) + a_{33}(Z - Z_s)} \quad [2]$$

where X, Y and Z are the ground coordinates, x and y are the image coordinates, X_s, Y_s and Z_s are the coordinates of the exposure centre in the ground coordinate system, f is the calibrated focal length of the camera, x_o and y_o are the image coordinates of the principle point, and a_{ij} are the elements of the rotation matrix with the three angles (ω, φ, k) (Omega, Phi and Kappa – yaw, pitch and roll). f, x_o and y_o represent the interior orientation parameters which were measured using the camera calibration report, while X_s, Y_s, Z_s, $\omega, \varphi,$ and k are the exterior orientation parameters (Nagarajan & Schenk 2016; Kaichang, Ruijin & Rong Xing 2003; Schenk 2004).

For this study, warped images necessitated manual interior orientation to align image and camera coordinates using the fiducial marks present on the images. Automatic tie point extraction was achieved using a combination of feature-based and least-squares matching procedures, but was only possible after the relative positions of the images in the block were refined by placing three manual tie points in *Von Gruber* positions for each image (Trimble/Inpho, 2014a).

Eight post-processing models were then tested using the results of the functional model used to triangulate each photo job (Table 2). The procedure started with a standard model run (std0.1), which included no blunder removal, no self-calibration and with fixed standard deviations set for planimetric and height ground control points (namely, 0.1m and 0.1m). This standard model run was then post processed using the seven different options described in Table 2.

2.2.3. Orthorectification

After each post-processing run, the exterior orientation for each photo job was imported into OrthoMaster. Orthographic corrections were performed using the Ortho Rectification tool and a 25m Digital Elevation Model (absolute accuracy 2.5 – 5m) (Trimble/Inpho 2014).

Table 2 A list of post-processing models that were selected and run to evaluate the success of aerial triangulation accuracy and final orthorectification accuracy.

Model name	**Self-calibration**	**Blunder removal**	**Eliminate manual points**	**Standard deviations gcp (planimetric, height [m])**	**Automatic and manual tie points**	**Standard deviations for automatic and manual tie points [μ (pixels)]**
std0.1	off	off	no	0.1, 0.1	yes	4 (0.2), 10 (0.5)
b0.1	off	radicle	yes	0.1, 0.1	yes	4 (0.2), 10 (0.5)
c0.1	44-parameters	off	no	0.1, 0.1	yes	4 (0.2), 10 (0.5)
cb0.1	44-parameters	radicle	yes	0.1, 0.1	yes	4 (0.2), 10 (0.5)
no-auto0.1	off	off	no	0.1, 0.1	manual only	4 (0.2), 10 (0.5)
std2-5	off	off	no	2, 5	yes	4 (0.2), 10 (0.5)
c2-5	44-parameters	off	no	2, 5	yes	4 (0.2), 10 (0.5)
cb2-5	44-parameters	radicle	yes	2, 5	yes	4 (0.2), 10 (0.5)

2.2.4. Accuracy assessment

For assessing final orthoimage planimetric accuracy, orthoimages generated in OrthoMaster and ground control points captured in the current orthoimage aerial triangulation project files were imported into ArcGIS. A manual procedure was then used to plot the deviation of each control point in the historical orthoimages from the ground control point in the current orthoimages (reference images). Deviations were measured for ground control points in all historical orthoimages including overlapping images. For example, for photo job 266 there were 40 ground control points with 117 photos covering at least one of these. The “deviation” is the root mean square error (RMSE) and can be expressed as follows:

$$RMSE_i = \sqrt{x_i^2 + y_i^2} \quad [3]$$

where i is each ground control point and x_i and y_i are the residuals in the x and y axes. The total root mean square error for each post-processing run was derived using the following equation.

$$Total\ RMSE = \sqrt{\frac{1}{n}\sum_{i=1}^{n} RMSE_i} \quad [4]$$

where $RMSE_i$ is the error associated with each ith ground control point (Rocchini et al. 2012). Planimetric accuracy was also assessed at checkpoints for all photo jobs but only for the top two performing models and the standard model run (std0.1).

Spearman rank correlations were then performed to investigate correlations between accuracy results from the aerial triangulation process (Table 3) and final planimetric accuracy (Table 4) of orthoimages generated (R Core Team 2016; Wei 2013; Wickham 2009; Harrell & Dupont 2015).

Table 3 Accuracy parameters generated in Inpho photogrammetric software for the aerial triangulation process with bundle block adjustment.

Abbreviation (in paper)	General name	Description	Ideal value
Sig0	Sigma0 [microns]	An overall accuracy result for the fit of the block considering manual and/or automatic points and ground control points (XYZ)	1/3 of a pixel (therefore 7.05µ for this study)
manual.x/y	RMS manual points in photo	Residuals in manual tie points for x and y	This should be roughly equal to the standard deviations set. The default standard deviations were used for this study (see Table 2)
auto.x/y	RMS automatic points in photo	Residuals in automatic tie points for x and y	
at.XY/Z	RMS control points	The total root mean square error of the residuals in meters of X, Y and Z ground control points	This should be less than or roughly equal to the standard deviations set for the project (see Table 2)
at.max.XY	Maximum RMS control points XY	The maximum root mean square error of the residuals in meters of X and Y ground control points	

Table 4 Accuracy assessment variables derived from manually measured deviations between historical orthoimages generated and reference orthoimages in ArcGIS.

Abbreviation (in paper)	General name	Description	Ideal value
or.XY	RMSE control points XY	The total root mean square error of residuals between ground control points in final historical orthoimages and current reference orthoimages.	As low as possible but dependent on study application. RMSE of ~ 10m have been achieved for other studies working in rugged terrain with <4 for more gentle terrain (Wang & Ellis 2005b; Rocchini et al. 2006, 2012)
Or.max.XY	Maximum RMSE control points XY	The maximum root mean square error found between ground control points in final historical orthoimages and current reference orthoimages	As low as possible but dependent on study application. ~15m has been achieved for other studies working in rugged terrain (Rocchini et al. 2012) .

3. Results and Discussion

3.1. Planimetric accuracy of orthoimages

The self-calibrated post-processing model, c0.1, consistently showed the highest final planimetric accuracy at ground control points for all four historical aerial photo jobs (Figure 4). This model can be viewed as achieving reasonably high accuracy especially given the limitations of the study area (complex geomorphology) and image quality (warpage across image surfaces) (Rocchini et al. 2012). The model also managed to retain this accuracy at additional checkpoints which were not included in the aerial triangulation process (Figure 5).

The non-automated model, which only included manual tie points (i.e. noauto0.1), showed the next highest accuracy at ground control for three of the photo jobs (226, 225 and 699). However, in contrast to the self-calibrated model, this model showed inconsistent planimetric accuracy with three out the four photo jobs showing decreased planimetric accuracy at additional checkpoints. In certain cases, this included an increase of more than 30 meters of planimetric error (Figure 5). Post-processing models that allowed the aerial triangulation process more room to adjust around ground control points (i.e. setting standard deviation of five and two meters) were ineffective at reducing the final root mean square errors in orthoimages. This is despite being a far more realistic standard deviation estimate. For example, it is rather unrealistic to assume the standard deviation for ground control digitised from an orthoimage as being within 10cm. Constraining the standard deviations, however, clearly resulted in higher planimetric accuracy.

3.2. Aerial triangulation accuracy compared with final planimetric accuracy

The overall aerial triangulation accuracy for most post-processing models was much lower than the recommended one third of a pixel. Average Sigma0 was 38µ (1.8 pixels) and ranged from 11µ (0.5 pixels) to 147µ (7 pixels) (see *AT Sig0* in red in Figure 4). Nonintuitively, the overall accuracy of the aerial triangulation process as measured by the Sigma0 was significantly negatively correlated with final planimetric accuracy at ground control (i.e. or.XY and or.max.XY) (Figure 6). A similar relationship was found for the residuals in automatic points x (auto.x), and no significant

correlations were found between all other aerial triangulation accuracy results and final planimetric accuracy in historical orthoimages (Figure 6).

When considering aerial triangulation accuracy results for ground control there were, again, no significant correlations present for post-processing models, which were set at a standard deviation of 0.1m (Figure 7 A). For more flexible models (standard deviation at 2m and 5m), a more positive relationship seemed to develop which included significant positive correlations between maximum planimetric accuracy in orthoimages (or.max.XY) and maximum aerial triangulation root mean square errors and residuals for height ground control (Figure 7 B). However, flexible models also showed the lowest final planimetric accuracy and therefore this is not an entirely useful measurement.

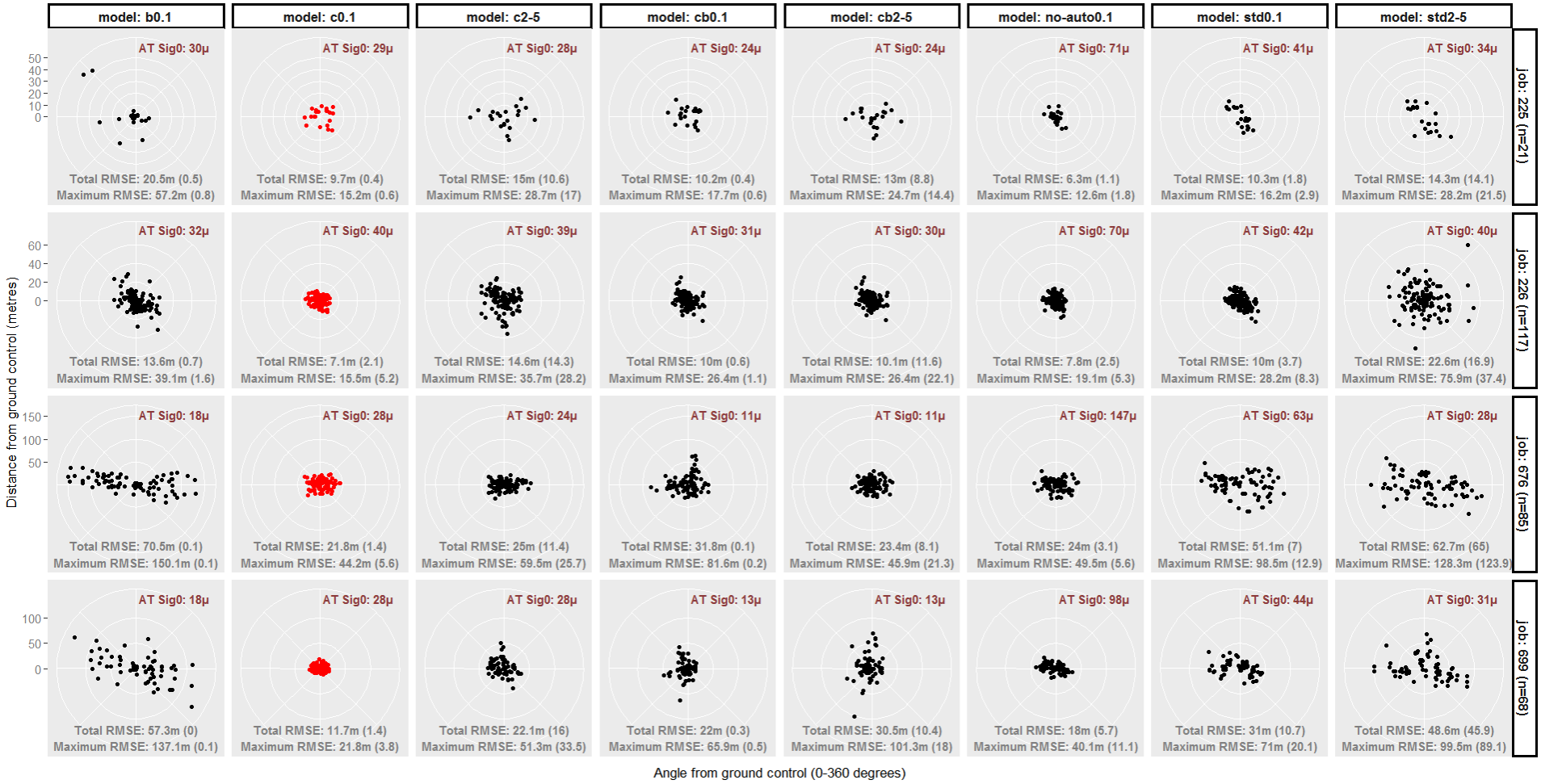

Figure 4 Final planimetric accuracy of orthoimages generated and direction of error for all ground control points summarised by the total and maximum root mean sqaure error (RMSE). Aerial triangulation accuracy measurements are included for comparison purposes including total and maximum XY root mean square error results shown in brackets and the overall triangulation accuracy in red (AT Sig0) .

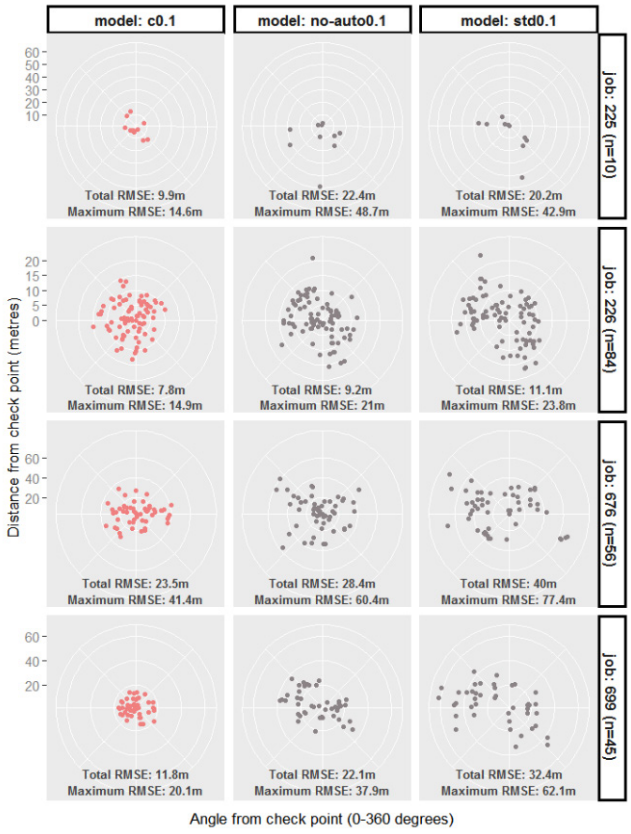

Figure 5 Final planimetric accuracy at check points for orthoimages for all four photo jobs for c0.1, no-auto0.1 and std0.1 post-processing models.

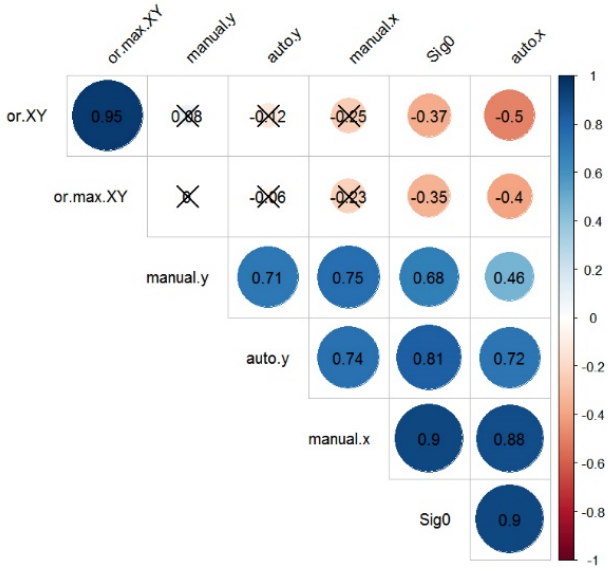

Figure 6 Spearman rank correlation coefficients between final orthoimage planimetric accuracy (or.XY and or.max.XY) and aerial triangulation accuracy measurements (Sig0, manual.x and manual.y, auto.x, auto.y). P values > 0.05 are indicated by a cross through the coefficient values.

A (n= 20): SD set at **0.1m**

B (n= 12): **2m and 5m** respectively

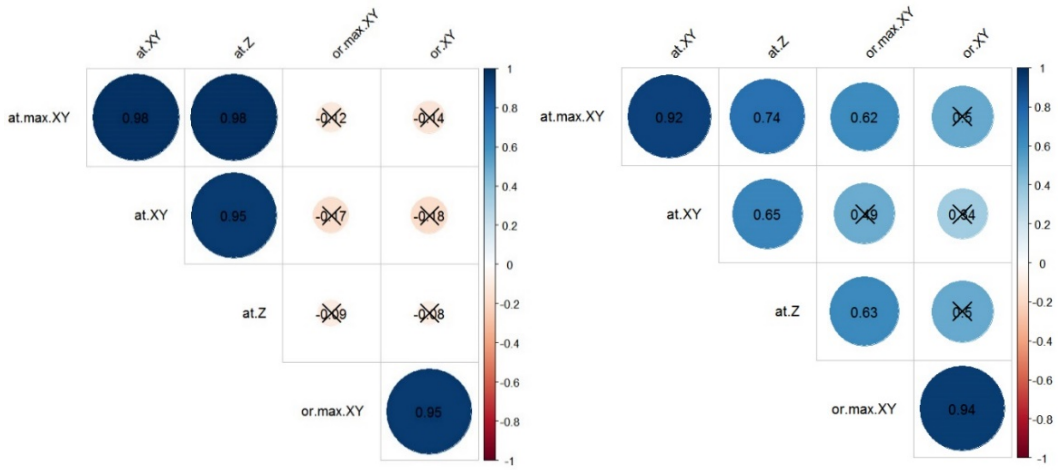

Figure 7 Spearman rank correlation coefficients between final orthoimage planimetric accuracy (or.) and aerial triangulation root mean sqaure errors (at.) at ground control grouped by standard deviation (SD) settings in corrplot A and corrplot B. P values > 0.05 are indicated by a cross through the coefficient values.

Limited and negative correlations between aerial triangulation results and final planimetric accuracy could be linked to a combination of aspects. Poor interior orientation (Figure 8) because of warpage and degradation across the entire image surface could have reduced the overall accuracy of the aerial triangulation process for all calibrated as well as non-calibrated post-processing models. It is also likely that the poor interior orientation process prevented a fully automated tie point matching process and the need for manually placing points in the *Von Gruber* positions for all images in all photo jobs. Poor interior orientation likely resulted in large residuals of the corresponding image and object coordinates. Therefore, although manually and automatically measured points were visually correctly measured, when using blunder detection they were eliminated because of poor transformation parameters of the interior orientation (Table 5). Furthermore, for post-processing models in which blunder detection was not used, the accuracy calculated for image and object coordinates was low, and this affected the overall Sigma0 and resulted in misalignment between aerial triangulation results and final planimetric accuracy in orthoimages.

Blunder detection removes observations based on standard deviations specified. The smaller the standard deviation specified the higher the weight and the more accurate observations have to be, not to be eliminated. The higher the standard deviation values, larger observation error is accepted and the observation will not be eliminated. Therefore, when blunder detection was used in combination with a standard deviation of 0.1m the process removed manually placed points (including ground control), which were correctly placed. This was then determined by the aerial triangulation model as an increase in accuracy whereby “incorrect” tie points or control points (which in fact were actually correct) had been removed. As a result, post-processing models, including blunder detection and fixed to the ground control showed some of the highest accuracy for the aerial triangulation process i.e. lower Sigma0 and ground control root mean square errors

(e.g. b0.1 and cb0.1). This however did not translate into similar levels of accuracy in the final orthoimages generated as achieved when using the self-calibrated model, c0.1, which showed lower aerial triangulation accuracy but higher final orthoimage planimetric accuracy at ground control (see b0.1 and c0.1 in Figure 4). One way of avoiding manual and automatic measurements from being eliminated is by giving them a larger standard deviation, thus allowing bigger residuals. However, post-processing models with planimetric and height standard deviations of five and two meters respectively did not achieve acceptable levels of final planimetric accuracy (Figure 4).

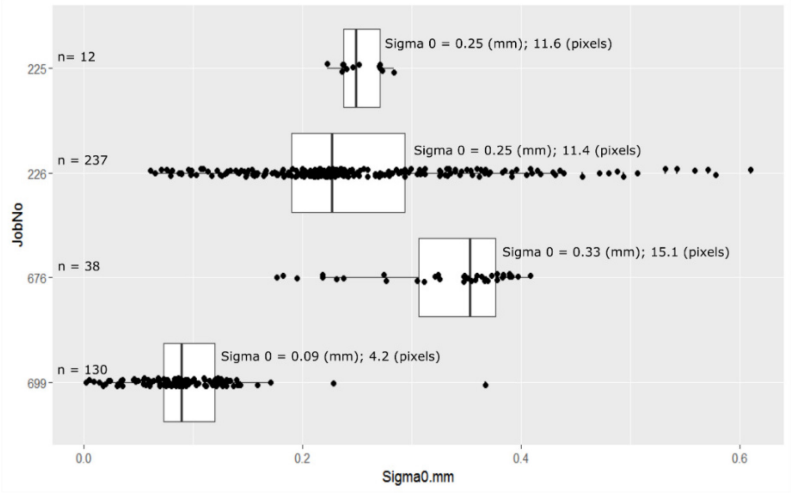

Figure 8 Boxplot of interior orientation results. Jitter points indicate individual images per photo job. The mean Sigma0 (in mm and pixels) is shown for each photo job.

Table 5 Ground control points, automatic tie and manual points for different model runs.

Photo job	**225**	**226**	**676**	**699**	**225**	**226**	**676**	**699**	**225**	**226**	**676**	**699**
post-processing model	**no. of ground control**				**no. of automatic tie points**				**no. of manual tie points**			
b0.1	6	13	3	4	887	26769	6106	16941	95	4063	397	1654
cb0.1	8	16	9	6	884	26773	5713	16558	97	4063	395	1595
cb2-5	9	40	30	21	884	26766	5755	16599	100	4078	453	1632
no-auto0.1	9	40	30	23	0	0	0	0	107	4521	521	1913
c0.1	9	40	30	23	891	26778	6419	17968	107	4521	521	1913
c2-5	9	40	30	23	891	26778	6419	17968	107	4521	521	1913
std0.1	9	40	30	23	891	26778	6419	17968	107	4521	521	1913
std2-5	9	40	30	23	891	26778	6419	17968	107	4521	521	1913

3.3. Discussion

Errors from warpage are cumulative during the aerial triangulation and orthorectification process. This study has shown however that it is not completely restrictive with certain post-processing models being able to achieve relatively acceptable accuracy. The self-calibration process in combination with constrained standard deviations of 0.1m consistently resulted in improved final planimetric accuracy across the four different photo jobs tested which included different ground control points, area coverage and number of images.

Although the process could not be fully automated, a substantially reduced number of ground control points was used in all photo jobs in comparison to the recommended 4-20 per image or image pair. For example, for a photo job of 237 images (covering ~150 000ha), this study used 40 ground control points and placed three manual tie points per image. Manual tie points between images were required, however, these are much quicker to find and measure in comparison to ground control points. Despite the assumed random nature of the error, self-calibration proved effective for increasing final planimetric accuracy to acceptable levels at both ground control and furthermore at additional check points indicating that there may have been some level of systematic error in the aerial images (Kaichang, Ruijin & Rong Xing 2003).

The total and maximum root mean square errors achieved for ground control and checkpoints for the constrained self-calibrated model, c0.1, are on par with orthorectification results achieved in other geomorphologically complex areas with higher quality original analogue photos and better scanning procedures (Rocchini et al. 2012). Local studies have a tendency to not report on georeferencing error with most dismissing the need for checkpoints and therefore rendering the total root mean square errors (when reported) an inadequate reflection of the positional error across the images. In studies that have reported errors, these have been relatively large, despite the flat terrain, ranging from ±15 – 30 meters (total RMSE) (Palmer et al. 2010; Keay-Bright & Boardman 2006; Wigley, Bond & Hoffman 2009, 2010; Buitenwerf et al. 2012; de Neergaard et al. 2005; Garden & Garland 2005; Giannecchini, Twine & Vogel 2007; Gordijn, Rice & Ward 2012; Grenfell et al. 2010; Higgins, Richardson & Cowling 2001; Hudak & Wessman 1998; Puttick, Hoffman & Gambiza 2011, 2014; Halpern & Meadows 2013; Corrigan et al. 2010).

When considering aerial triangulation of historical aerial imagery, it is important to understand that high aerial triangulation accuracy does not always translate into high planimetric accuracy in final orthoimages generated. Aerial triangulation accuracy results are highly influenced by the standard deviations set as well as other post-processing parameters linked to blunder detection and calibration. It is possible that the addition of more manual tie points for post-processing models that do not include blunder detection could reduce final planimetric errors in orthoimages. However, this would likely reduce the aerial triangulation accuracy results, an artefact of the post-processing model assuming manually placed points are incorrectly placed because of poor interior orientation, but also increase the time required for each independent photo job. The influence of the accuracy and number of points in the control network is a theme for further research.

4. Conclusion

This study has shown that automatic aerial triangulation can be used for orthorectifying historical aerial photos with a reduced number of ground control for large blocks of aerial imagery. Self-calibration in conjunction with constraining standard deviations around the ground control was required for achieving acceptable levels of planimetric accuracy in final orthoimages comparable to other studies working in geomorphologically complex areas as well as an improvement to georeferencing studies in South Africa.

The national mapping department in South Africa has an extensive collection of historical analogue aerial photos with a large coverage across the country dating from the early 1900s (Figure 2). This is not unique to South Africa with many other countries (including least developed and developing) also having extensive analogue photos in storage (Palandro et al. 2003; Tekle & Hedlund 2000; Schiefer & Gilbert 2007). Ideally, imagery could be provided on an open source platform ready for viewing by the public and for review for potential change detection studies by applied scientists and other researchers. GeoMemories is an example of an initiative working towards this goal in the Italian landscape (Abrate et al. 2013). Libraries of Brock University, Santa Barbara and Stanford Universities have also been conducting similar work towards creating portals for national aerial photo archival data collection and distribution (Ma & Buchwald 2012).

5. Acknowledgements

NGI contributed the scanning of analogue aerial photos. Raoul Duesimi (NGI) assisted with access to storage areas and provided Intergraph aerial triangulation project files of current orthoimages and the data for generating Figure 2. Additional individuals that assisted and supported the study at NGI include Sue Kirschner, Rabelani Lidzhade and Aslam Parker. Maps throughout this article were created using ArcGIS® software by Esri. The research was funded by the Plant Conservation Unit, the African Climate Development Initiative and the National Research Foundation.

6. References

Abrate, M, Bacciu, C, Hast, A, Marchetti, A, Minutoli, S & Tesconi, M 2013, "GeoMemories-A platform for visualizing historical, environmental and geospatial changes in the Italian landscape," *ISPRS International Journal of Geo-Information*, vol. 2, no. 2, p. 432.

Addo, KA 2010, "Urban and peri-urban agriculture in developing countries studied using remote sensing and in situ methods," *Remote Sensing*, vol. 2, no. 2, pp. 497–513.

Asiyanbola, RA 2014, "Remote sensing in developing country-Nigeria: An exploration," *Journal of Geography and Geology*, vol. 6, no. 1, pp. 110–128.

Bianchetti, RA & MacEachren, AM 2015, "Cognitive themes emerging from air photo interpretation texts Published to 1960," *ISPRS International Journal of Geo-Information*, vol. 4, no. 2, pp. 551–571.

Buitenwerf, R, Bond, W, Stevens, N & Trollope, W 2012, "Increased tree densities in South African savannas: > 50 years of data suggests CO2 as a driver," *Global Change Biology*, vol. 18, no. 2, pp. 675–684.

Chen, J, Dowman, I, Li, S, Li, Z, Madden, M, Mills, J, Paparoditis, N, Rottensteiner, F, Sester, M, Toth, C, Trinder, J & Heipke, C 2016, "Information from imagery: ISPRS scientific vision and research agenda," *ISPRS Journal of Photogrammetry and Remote Sensing*, vol. 115, pp. 3–21.

Corrigan, B, Kneen, M, Geldenhuys, C & van Wyk, B 2010, "Spatial changes in forest cover on the KwaNibela Peninsula, St Lucia, South Africa, during the period 1937 to 2008," *Southern Forests: A Journal of Forest Science*, vol. 72, no. 1, pp. 47–55.

DEA 2016, *[Vector geospatial data]. South Africa Protected Areas Database (SAPAD_OR_2016_Q2)*, Department of Environmental Affairs, Enterprise Geospatial Information Management, Pretoria, South Africa. Accessed online from http://egis.environment.gov.za (December 2015).

ESRI 2015, *ArcGIS for desktop 10.3*, Environmental Systems Research Institute, Redlands, CA. www.esri.com.

Garden, S & Garland, G 2005, "Spit development in the Mdloti River estuary, KwaZulu-Natal," *South African Journal of Geology*, vol. 108, no. 2, pp. 257–270.

Gennaretti, F, Ripa, MN, Gobattoni, F, Boccia, L & Pelorosso, R 2011, "A methodology proposal for land cover change analysis using historical aerial photos," *Journal of Geography and Regional Planning*, vol. 4, no. 9, pp. 542–556.

Giannecchini, M, Twine, W & Vogel, C 2007, "Land-cover change and human-environment interactions in a rural cultural landscape in South Africa," *The Geographical Journal*, vol. 173, no. 1, pp. 26–42.

Gordijn, PJ, Rice, E & Ward, D 2012, "The effects of fire on woody plant encroachment are exacerbated by succession of trees of decreased palatability," *Perspectives in Plant Ecology, Evolution and Systematics*, vol. 14, no. 6, pp. 411–422.

Grenfell, SE, Ellery, WN, Grenfell, MC, Ramsay, LF & Fluegel, TJ 2010, "Sedimentary facies and geomorphic evolution of a blocked-valley lake: Lake Futululu, northern Kwazulu-Natal, South Africa," *Sedimentology*, vol. 57, no. 5, pp. 1159–1174.

Halpern, A & Meadows, M 2013, "Fifty years of land use change in the Swartland, Western Cape, South Africa: characteristics, causes and consequences," *South African Geographical Journal*, vol. 95, no. 1, pp. 38–49.

Harrell, F & Dupont, C 2015, *Hmisc: Harrell Miscellaneous*, R package version 3.17-1, https://CRAN.R-project.org/package=Hmisc (June 2016).

Higgins, SI, Richardson, DM & Cowling, RM 2001, "Validation of a spatial simulation model of a spreading alien plant population," *Journal of Applied Ecology*, vol. 38, no. 3, pp. 571–584.

Hudak, AT & Wessman, CA 1998, "Textural analysis of historical aerial photography to characterize woody plant encroachment in South African savanna," *Remote Sensing of Environment*, vol. 66, no. 3, pp. 317–330.

Hughes, ML, McDowell, PF & Marcus, WA 2006, "Accuracy assessment of georectified aerial photographs: implications for measuring lateral channel movement in a GIS," *Geomorphology*, vol. 74, no. 1, pp. 1–16.

Kaichang, D, Ruijin, M & Rong Xing, L 2003, "Rational functions and potential for rigorous sensor model recovery," *Photogrammetric Engineering & Remote Sensing*, vol. 69, no. 1, pp. 33–41.

Keay-Bright, J & Boardman, J 2006, "Changes in the distribution of degraded land over time in the central Karoo, South Africa," *Catena*, vol. 67, no. 1, pp. 1–14.

Linder, W 2006, *Digital photogrammetry. 1st edition*, Springer, Netherlands.

Ma, R & Buchwald, A 2012, "Orthorectify historical aerial photographs using DLT," in ASPRS, Sacramento, California.

Marignani, M, Rocchini, D, Torri, D, Chiarucci, A & Maccherini, S 2008, "Planning restoration in a cultural landscape in Italy using an object-based approach and historical analysis," *Landscape and Urban Planning*, vol. 84, no. 1, pp. 28–37.

MDB 2013, *[Vector geospatial data]. South Africa provinces boundary data main files*, Municipal Demarcation Board. Accessed online from http://www.demarcation.org.za/ (December 2015).

Morgan, JL, Gergel, SE & Coops, NC 2010, "Aerial photography: a rapidly evolving tool for ecological management," *BioScience*, vol. 60, no. 1, pp. 47–59.

Nagarajan, S & Schenk, T 2016, "Feature-based registration of historical aerial images by Area Minimization," *ISPRS Journal of Photogrammetry and Remote Sensing*, vol. 116, pp. 15–23.

De Neergaard, A, Saarnak, C, Hill, T, Khanyile, M, Berzosa, AM & Birch-Thomsen, T 2005, "Australian wattle species in the Drakensberg region of South Africa - An invasive alien or a natural resource?," *Agricultural Systems*, vol. 85, no. 3, pp. 216–233.

NGI 2015a, *[Vector geospatial data]. Photo coverages. All 498 Jobs*, National Geospatial Institution (NGI), a component of the Department of Rural Development and Land Reform (DRDLR), Accessed from NGI, Mowbray, South Africa (July 2015).

NGI 2015b, *[Vector geospatial data]. Photo coverages. All Standard Jobs*, National Geospatial Institution (NGI), a component of the Department of Rural Development and Land Reform (DRDLR), Accessed from NGI, Mowbray, South Africa (July 2015).

NGI-DEM 2016, *[Digital elevation model]. A photogrammetrically compiled Digital Elevation Model of South Africa with an absolute accuracy of 2-5m and resolution of 25m*, National Geospatial Institution (NGI), a component of the Department of Rural Development and Land Reform (DRDLR), Mowbray, South Africa.

Palandro, D, Andréfouët, S, Dustan, P & Muller-Karger, F 2003, "Change detection in coral reef communities using Ikonos satellite sensor imagery and historic aerial photographs," *International Journal of Remote Sensing*, vol. 24, no. 4, pp. 873–878.

Palmer, BJ, McGregor, GK, Hill, TR & Paterson, AW 2010, "A spatial assessment of coastal development and land use change in the Eastern Cape, South Africa," *South African Geographical Journal*, vol. 92, no. 2, pp. 117–128.

Pulighe, G & Fava, F 2013, "DEM extraction from archive aerial photos: accuracy assessment in areas of complex topography," *European Journal of Remote Sensing*, vol. 46, pp. 363–378.

Puttick, J, Hoffman, M & Gambiza, J 2011, "Historical and recent land-use impacts on the vegetation of Bathurst, a municipal commonage in the Eastern Cape, South Africa," *African Journal of Range & Forage Science*, vol. 28, no. 1, pp. 9–20.

Puttick, JR, Hoffman, MT & Gambiza, J 2014, "The impact of land use on woody plant cover and species composition on the Grahamstown municipal commonage: implications for South Africa's land reform programme," *African Journal of Range & Forage Science*, vol. 31, no. 2, pp. 123–133.

R Core Team 2016, *R: A language and environment for statistical computing*, R Foundation for Statistical Computing, Vienna, Austria. URL https://www.R-project.org/.

Rocchini, D 2004, "Misleading information from direct interpretation of geometrically incorrect aerial photographs," *The photogrammetric record*, vol. 19, no. 106, pp. 138–148.

Rocchini, D, Metz, M, Frigeri, A, Delucchi, L, Marcantonio, M & Neteler, M 2012, "Robust rectification of aerial photographs in an open source environment," *Computers & Geosciences*, vol. 39, pp. 145–151.

Rocchini, D, Perry, GL, Salerno, M, Maccherini, S & Chiarucci, A 2006, "Landscape change and the dynamics of open formations in a natural reserve," *Landscape and Urban Planning*, vol. 77, no. 1, pp. 167–177.

Rocchini, D & Di Rita, A 2005, "Relief effects on aerial photos geometric correction," *Applied Geography*, vol. 25, no. 2, pp. 159–168.

De Rose, RC & Basher, LR 2011, "Measurement of river bank and cliff erosion from sequential LIDAR and historical aerial photography," *Geomorphology*, vol. 126, no. 1, pp. 132–147.

Schenk, T 1996, "Digital aerial triangulation," *International Archives of Photogrammetry and Remote Sensing*, vol. 31, pp. 735–745.

Schenk, T 2004, "From point-based to feature-based aerial triangulation," *ISPRS Journal of Photogrammetry and Remote Sensing*, vol. 58, no. 5, pp. 315–329.

Schiefer, E & Gilbert, R 2007, "Reconstructing morphometric change in a proglacial landscape using historical aerial photography and automated DEM generation," *Geomorphology*, vol. 88, no. 1, pp. 167–178.

SUDEM 2014, *[Digital elevation model]. 5m resolution hillshade of South Africa*, University of Stellenbosch. ArcGIS. Version 10.3. Environmental Systems Research Institute, Redlands, CA. (April 2016).

Tekle, K & Hedlund, L 2000, "Land cover changes between 1958 and 1986 in Kalu District, southern Wello, Ethiopia," *Mountain Research and Development*, vol. 20, no. 1, pp. 42–51.

Trimble/Inpho 2014, *[Precision Photogrammetry and Digital Modelling Software]. Application Master, MATCH-AT and OrthoMaster software packages*, Inpho Version 7.0. Trimble, Germany.

Verhoeven, G, Doneus, M, Briese, C & Vermeulen, F 2012, "Mapping by matching: a computer vision-based approach to fast and accurate georeferencing of archaeological aerial photographs," *Journal of Archaeological Science*, vol. 39, no. 7, pp. 2060–2070.

Wang, H & Ellis, E 2005a, "Image misregistration error in change measurements," *Photogrammetric Engineering & Remote Sensing*, vol. 71, no. 9, pp. 1037–1044.

Wang, H & Ellis, E 2005b, "Spatial accuracy of orthorectified IKONOS imagery and historical aerial photographs across five sites in China," *International Journal of Remote Sensing*, vol. 26, no. 9, pp. 1893–1911.

Wei, T 2013, *corrplot: Visualization of a correlation matrix*, R package version 0.73. https://CRAN.R-project.org/package=corrplot.

Wickham, H 2009, *Ggplot2: Elegant graphics for data analysis*, Springer-Verlag, New York.

Wigley, B, Bond, W & Hoffman, M 2009, "Bush encroachment under three contrasting land-use practices in a mesic South African savanna," *African Journal of Ecology*, vol. 47, no. s1, pp. 62–70.

Wigley, BJ, Bond, WJ & Hoffman, M 2010, "Thicket expansion in a South African savanna under divergent land use: local vs. global drivers?," *Global Change Biology*, vol. 16, no. 3, pp. 964–976.